Short wavelength infrared optical windows for evaluation of benign and malignant tissues

Diana C. Sordillo
Laura A. Sordillo
Peter P. Sordillo
Lingyan Shi
Robert R. Alfano

SPIE.

Short wavelength infrared optical windows for evaluation of benign and malignant tissues

Diana C. Sordillo,[a] **Laura A. Sordillo,**[a,b,*] **Peter P. Sordillo,**[a,c] **Lingyan Shi,**[a,d] **and Robert R. Alfano**[a,b]
[a]Institute for Ultrafast Spectroscopy and Lasers, Department of Physics, City College of New York, New York, New York, United States
[b]The Grove School of Engineering, Department of Electrical Engineering, City College of New York, New York, New York, United States
[c]Lenox Hill Hospital, Department of Hematology and Oncology, New York, New York, United States
[d]Columbia University, Department of Chemistry, New York, New York, United States

Abstract. There are three short wavelength infrared (SWIR) optical windows outside the conventionally used first near-infrared (NIR) window (650 to 950 nm). They occur in the 1000- to 2500-nm range and may be considered second, third, and fourth NIR windows. The second (1100 to 1350 nm) and third windows (1600 to 1870 nm) are now being explored through label-free linear and multiphoton imaging. The fourth window (2100 to 2350 nm) has been mostly ignored because of water absorption and the absence of sensitive detectors and ultrafast lasers. With the advent of new technology, use of window IV is now possible. Absorption and scattering properties of light through breast and prostate cancer, bone, lipids, and intralipid solutions at these windows were investigated. We found that breast and prostate cancer and bone have longer total attenuation lengths at NIR windows III and IV, whereas fatty tissues and intralipid have longest lengths at windows II and III. Since collagen is the major chromophore at 2100 and 2350 nm, window IV could be especially valuable in evaluating cancers and boney tissues, whereas windows II and III may be more useful for tissues with high lipid content. SWIR windows may be utilized as additional optical tools for the evaluation of collagen in tissues. © *2017 Society of Photo-Optical Instrumentation Engineers (SPIE)* [DOI: 10.1117/1.JBO.22.4.045002]

Keywords: fourth NIR window; third optical window; short wavelength infrared; light scattering; collagen.

Paper 160708PR received Oct. 18, 2016; accepted for publication Mar. 3, 2017; published online Apr. 3, 2017.

1 Introduction

Near-infrared (NIR) spectroscopy (650 to 950 nm) has become an important modality for imaging and medical diagnostics, with applications that include cancer detection, assessing changes in tumors, measurement of blood flow to the brain, and evaluation of patients with Paget's disease of bone.[1–7] Short wavelength infrared (SWIR) spectroscopy, with wavelengths from 1000 to 2500 nm, may offer better penetration into turbid media, while minimizing radiation exposure. Biomolecules in tissue, such as oxyhemoglobin, hemoglobin, and water, have distinct absorption spectral patterns, thus they give optical fingerprints. The SWIR optical windows, which correspond to second, third, and fourth windows in the 1000- to 2500-nm wavelength range, occur between water absorption peak maxima and can reveal the presence of lipids, fats, glucose, and collagen, as well as of many other molecules, due to their distinct optical absorption spectral profiles.

Water absorption, as well as light scattering, limits the information collected by a detector. Rayleigh scattering is known to decrease with longer wavelength, varying as $1/\lambda^4$. Mie scattering will also decrease [varying as $1/\lambda^n$ for $n \geq 1$, where n varies with particle size for μ_s, not for reduced scattering coefficient $\mu_s' = \mu_s(1 - g)$]. Details on Mie scattering are available elsewhere.[8] Because of this, the utilization of SWIR wavelengths could present the opportunity to study chromophores beyond the conventional, first, NIR window.[9–11] Utilizing SWIR wavelengths can result in decreased scattering, might allow for less blurring, and result in better penetration into the tissue media; therefore, better contrast images might be obtained. Recently, NIR windows II (located between water peak maxima at 970 and 1444 nm) and III (located between water peak maxima of 1444 and 1950 nm) have been used for medical applications, such as *in vivo* imaging of small animals and the detection and monitoring of intestinal ischemia *in vivo* in a porcine model.[9–13] Window II occurs between 1100 and 1350 nm and window III between 1600 and 1870 nm. Window III has been referred to as the "golden window."[12]

A fourth NIR window, occurring between 2100 and 2350 nm (shown in Fig. 1), has been mostly ignored because of greater absorption by water at these wavelengths. However, Yoo et al. have shown that a small amount of absorption can limit the detection of diffusive photons, which may cause a blurring of images, and can highlight the ballistic and snake photons, which are responsible for producing clearer images.[14] Indeed, water absorption is less at shorter NIR wavelengths, but, due to the inverse wavelength dependence, scattering is minimal; this may result in a balance between absorption and scattering events. The fourth NIR window has also been discounted due to a lack of sensitive detectors. The advent of new photodetectors and laser sources now makes window IV a viable spectral domain (Table 1). The photodetector of choice in window IV is InSb (either as single and array photodiodes). Ultrafast lasers that utilize wavelengths from window IV include the supercontinuum laser, with spectral range from 400 to 2500 nm, the

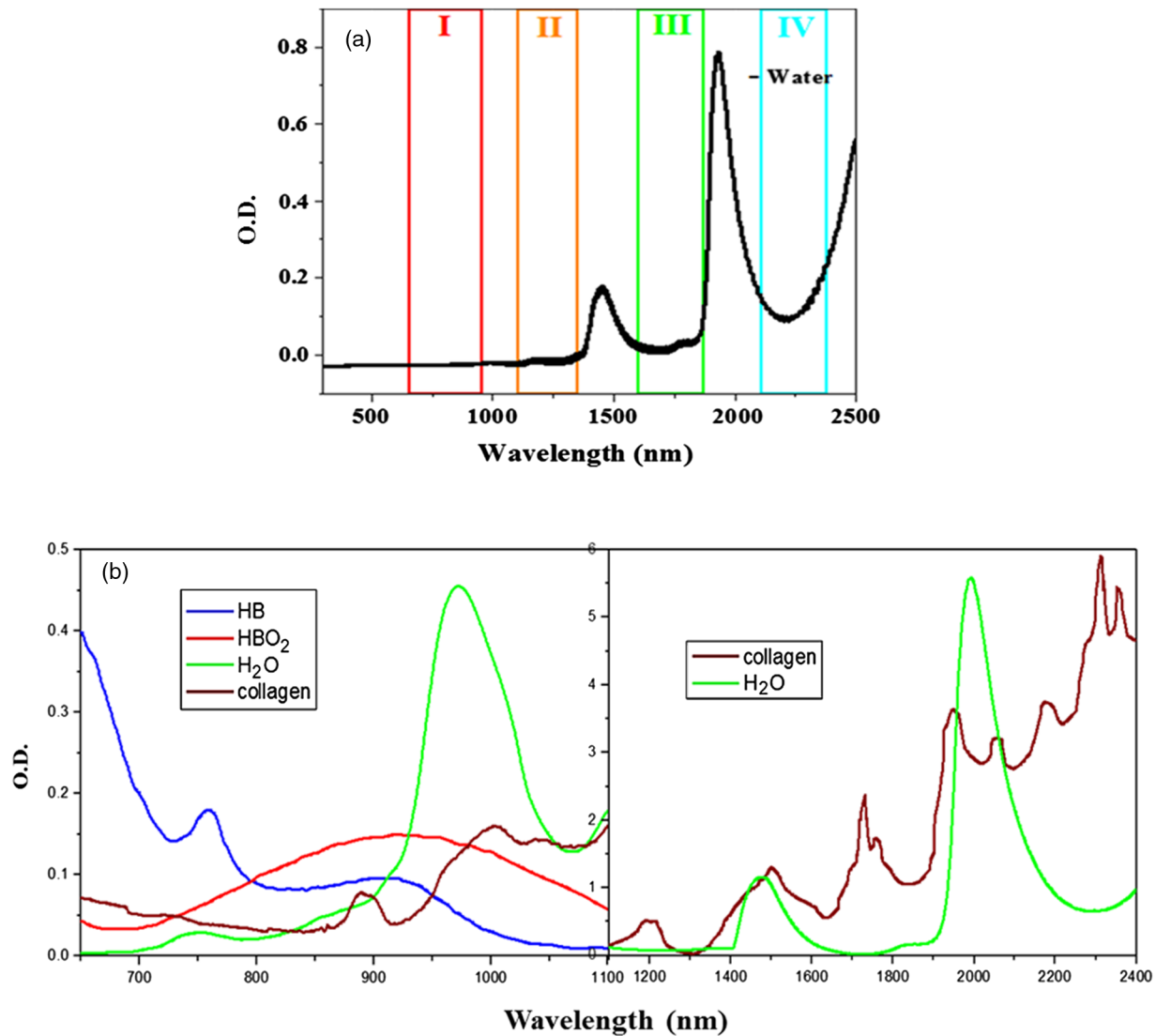*Address all correspondence to: Laura A. Sordillo, E-mail: lsordillo@ccny.cuny.edu

Fig. 1 (a) Optical density (O.D.) spectrum of water molecules in the NIR spectral range; (b) OD spectra of collagen and water at the first NIR and the three SWIR windows.[11]

Table 1 Ultrafast and continuous wave (CW) laser light sources for window III and IV.

Type	Wavelength range (nm)	Brand
Supercontinuum source	~400 to 2500 nm	Leukos, NKT Photonics, Thorlabs
Er:YAG laser	1645 nm	IPG Photonics
"Bodega" femtosecond optical parametric laser (FLOPA)	~1700 nm	Calmar
Cr^{2+}:ZnSe/S CW lasers	1800 to 3400 nm	IPG Photonics
GaSb laser diode lasers	1870 to 2230 nm	DILAS
GaSb-based laser diodes	1800 to 3000	Brolis semiconductors

Cr 2+:ZnSe/S lasers, and GaSb laser diodes.[15,16] Femtosecond Cr2+-doped ZnS and ZnSe lasers can be used at wavelengths from 1800 to 3400 nm, with Kerr mode locking that can generate ultrashort (41 fs) pulses. Room-temperature Cr2+-based lasers can provide tens of Watts of power and ultrabroad tunability (~1400 nm between 2 and 3.4 μm).[16] GaSb laser diodes are available from 1800 to 3000 nm. Brolis semiconductors now offer 2100 and 2200 nm GaSb diode lasers for SWIR microscopes. In window III, the 200-fs laser from Calmar [called Bodega femtosecond optical parametric laser (FLOPA)] is available at ~1700 nm. Recently, Sordillo et al. reported on the use of the fourth NIR window for the assessment of bone, at the 2016 SPIE Photonics West Conference.[17] As an extension of our work, we have measured the absorbance and have calculated the total attenuation lengths from lipid or collagen rich tissues, including breast and prostate cancer, bone, lipids, and intralipid solutions, at the first NIR and SWIR windows. The molecules that absorb by excitation of combination vibrations in the SWIR are presented.

2 Methods

The absorbance spectra from the samples were acquired using the UV–vis–NIR Cary 500 spectrophotometer (Varian, Inc., Palo Alto, California). The Cary 500 is a commercially available, research grade, spectrophotometer with a PbS detector, a deuterium arc UV lamp, and a tungsten halogen visible light. To produce a narrow band, nearly monochromatic, light beam, light from these sources is diffracted using a grating. This light is then allowed to hit the sample, which is placed at a fixed position in the sample compartment. Finally, optical density (OD) or percent transmission of light through the sample is recorded on the computer. These conditions were kept constant for all samples. The wavelength range was between 600 and 2500 nm, covering the first NIR and the SWIR ranges. Total attenuation lengths (l_t) were measured in windows I ($\lambda = 750$ nm), II ($\lambda = 1200$ nm), III ($\lambda = 1700$ nm), and IV ($\lambda = 2200$ nm). A sample of cleaned human fibula was obtained from a cadaver and cut to ~150 μm. 20% intralipid was diluted to concentrations of 0.5%, 1%, 1.5%, and 2%. Tissue samples were purchased from National Disease Research Interchange and Cooperative Human Tissue Network after approval by an institutional review board. The samples were neither fixed nor treated chemically. Samples were cut to thicknesses of ~50, 100, and 200 μm.

3 Theoretical Background

Light through turbid media is described by the trajectories of three components: diffusive, ballistic, and quasiballistic (snake) photons.[8,18] When the media is thin, the decay of ballistic photons (I_b) is described by the differential equation:[19]

$$dI_b/dz = -\mu_t I_b \tag{1}$$

with the solution

$$I_b = I_0 \exp(-\mu_t z), \tag{2}$$

where μ_t, the total attenuation coefficient, is defined as the sum of the absorption coefficient μ_a and the scattering coefficient $\mu_s (\mu_t = \mu_a + \mu_s)$, I_0 is the incident light (light entering the media), and z is the tissue thickness. Equation (2) is known as Beer–Lambert's law.

For thicker media, the diffusive photons (I_d) are governed by the diffusion equation, which can be approximated by[19]

$$\frac{\partial^2 I_d}{\partial z^2} = 3(\mu_s' + \mu_a)\mu_a I_d \tag{3}$$

with the solution

$$I_d = I_0 \exp\left[-(\sqrt{3\mu_a(\mu_s' + \mu_a)}z\right], \tag{4}$$

where $\mu_s' = \mu_s(1 - g)$ is the reduced scattering coefficient, $l_{tr} = 1/\mu_s'$ is defined as the transport mean-free path,[20] and $g = \langle \cos\theta \rangle$ is the mean cosine of the scattering angle (anisotropy factor).[21]

When the solid angle $\delta\Omega$ is small, the total transmitted light intensity I can be written as the sum of the number of ballistic photons (I_b) and of a fraction of the diffusive photons (I_d)[22]

$$I = I_b + \left(\frac{\delta\Omega}{4\pi}\right)I_d. \tag{5}$$

Substituting Eqs. (2) and (4) into Eq. (5) and dividing by I_0[23] we obtain

$$\frac{I}{I_0} = \exp(-\mu_t z) + \left(\frac{\delta\Omega}{4\pi}\right) \exp\left[-(\sqrt{3\mu_a(\mu_s' + \mu_a)}z\right]. \tag{6}$$

Yoo et al. have studied photon transport through random media utilizing ultrafast laser pulses and time-resolved detection.[14,24] The authors showed that for $z/l_{tr} < 10$, the diffusion approximation deviated monotonically from the measured scattered pulse, and that scattered photons arrived earlier than the diffusion approximation had predicted. Zhang et al. found that, at $z/l_{tr} \sim 3$, there is a sharp transition from ballistic to diffusive behavior.[25] The thickness z_c where the ballistic and diffusive photons are equal is given as[19]

$$z_c \equiv \frac{1}{\mu_s - \mu_{eff}} \ln\left(\frac{4\pi}{\delta\Omega}\right), \tag{7}$$

for $\mu_{eff} = \sqrt{3\mu_a(\mu_s' + \mu_a)}$. When $z < z_c$, the ballistic photons will govern over the diffusive ones; therefore, using tissue samples (<1 mm) will allow for better image quality.

4 Results

The measured percent transmission intensities and corresponding OD through a sample of human fibula using the four windows are plotted in Figs. 2(a) and 2(b). From these plots, the total attenuation coefficient (μ_t) obtained from the bone sample is calculated using Beer–Lambert's law

$$T = \frac{I}{I_0} = \exp[-(\mu_t z)]. \tag{8}$$

The total attenuation length (l_t) is the inverse of the total attenuation coefficients (μ_t) and is acquired by substituting $\mu_t = 1/l_t$ into the above equation

$$l_t = -z/\ln(T). \tag{9}$$

Figures 3(a) and 3(b) show the spectrum of the total attenuation coefficients (μ_t) and the spectrum of total attenuation lengths (l_t) from bone. Longest relative total attenuation lengths occur at wavelengths within the third and fourth windows. A salient feature is an oscillating structure about window IV. These spectra reveal small oscillations at wavelengths above 1800 nm, which are most likely due to the vibrational combination modes from collagen.

Figure 4 shows the spectra obtained from different concentrations of intralipid solution. For 0.5% and 1% intralipid solution, longest total attenuation lengths occur at window II. For 1.5% and 2% intralipid solution, longest total attenuation lengths are seen at window III. For 20% intralipid, longest total attenuation lengths occur at the third and fourth windows. Similarly, longest total attenuation lengths for both prostate and breast tissues are seen at window III. The oscillation in absorption plots beyond 1800 nm is attributed to collagen and lipids [see Fig. 1(b)]. Table 2 shows l_t for tissues with high collagen. Table 3 shows total attenuation lengths for chicken fat and for intralipid solution of different concentrations.
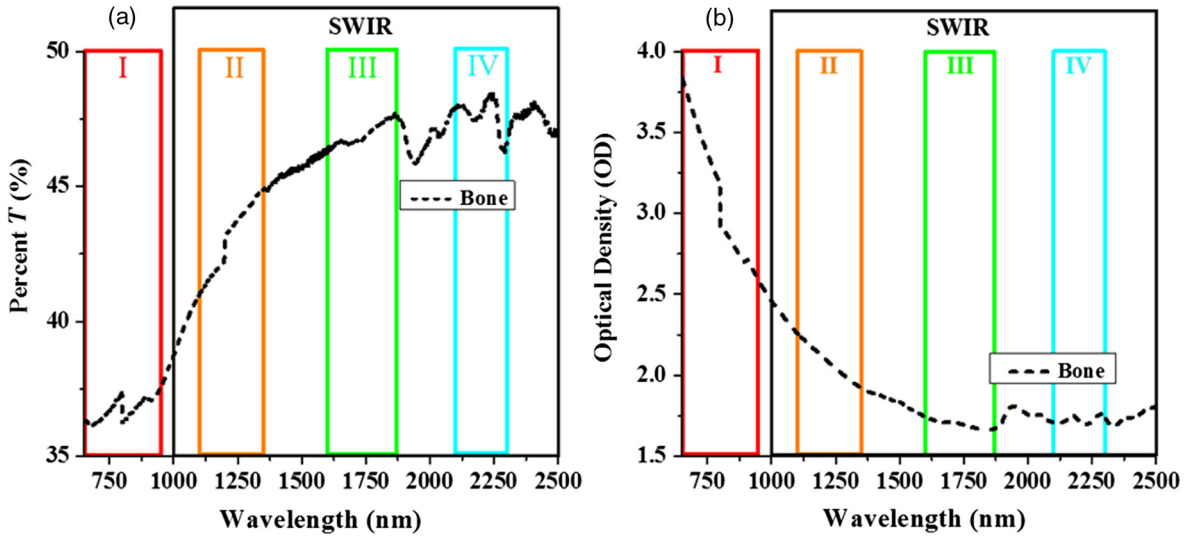
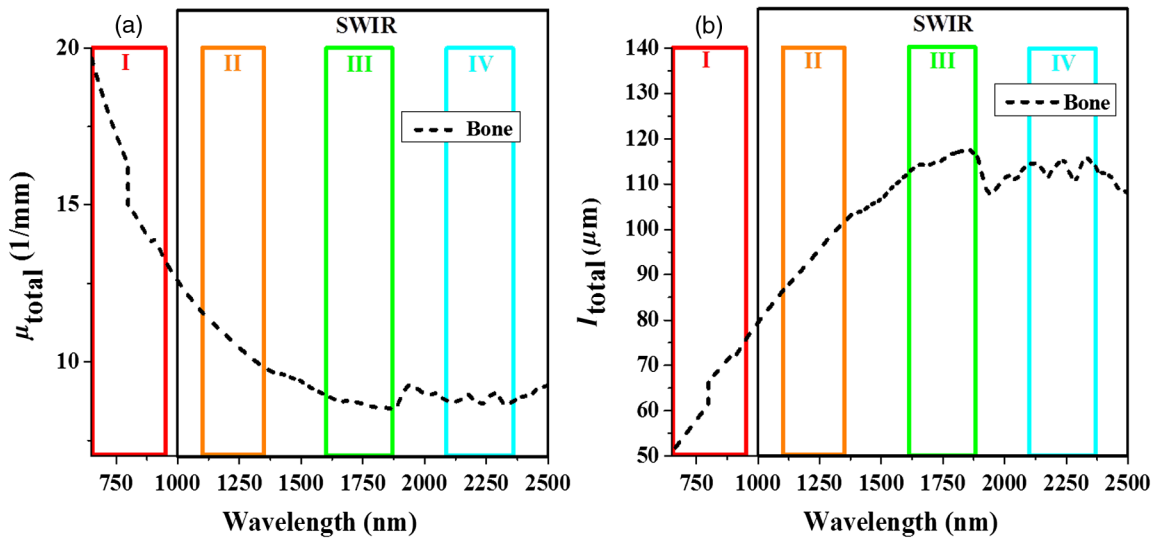**Fig. 2** (a) Percent transmission (T) and (b) OD spectra from a bone sample.

Fig. 3 (a) Total attenuation coefficients (μ_{total}) and (b) total attenuation lengths (l_{total}).
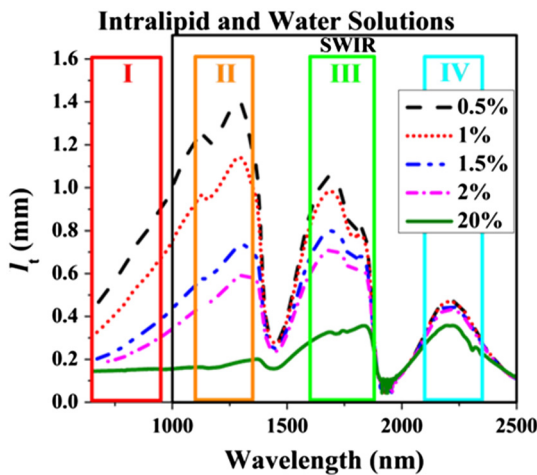

Fig. 4 l_t for 0.5%, 1%, 1.5%, 2%, and 20% concentrations of intralipid solution.

5 Discussion

Limited studies have been done utilizing wavelengths in the SWIR range, especially wavelengths above 2000 nm. Using samples of human skin, Troy et al. have reported the absorption and reduced scattering coefficients obtained at wavelengths between 1000 and 2200 nm. However, at wavelengths from 1900 to 2050 nm, the coefficients were not calculated because of increased water absorption (peak at $\lambda = 1920$ nm).[26] These authors also determined that, for wavelengths less than 1800 nm, a 2% intralipid solution was an appropriate skin tissue phantom. For wavelengths greater than 2100 nm, a 2% to 4% intralipid solution would be an appropriate phantom. Zamora-Rojas et al. investigated porcine skin in the SWIR range from 1150 to 2250 nm.[27] Due to a large water band, the authors could not obtain absorption coefficients in the spectral range from 1880 to 2040 nm but otherwise showed that scattering decreased with increasing SWIR wavelengths. Wang et al. looked at samples of human carotid atherosclerotic plaque at

Table 2 Total attenuation lengths from high collagen tissues at the first NIR and the SWIR optical windows.

Specimen	Thickness (μm)	Total attenuation lengths l_t (μm)			
		I	II	III	IV
Bone	150	58	92	114	114
Human prostate cancer	100	161	168	206	209
	200	101	159	217	213
Human breast cancer (patient 1)	100	169	311	438	365
	200	66	75	86	86
Human breast cancer (patient 2)	50	23	30	33	33
	100	66	99	127	132
	200	79	105	117	101
Human breast cancer (patient 3)	200	39	42	40	32
	200	49	51	56	52
Human breast cancer (patient 4)	200	75	83	84	72
	200	51	66	73	61
	200	171	184	170	176
Human breast cancer (patient 5)	200	167	182	214	255
	200	143	154	173	193
	200	73	76	96	119
Human breast cancer (patient 6)	200	102	104	133	162
	200	1348	2012	622	607

Table 3 Total attenuation lengths of chicken fat and of solutions of intralipid at the first NIR and the SWIR optical windows.

Tissue details		Total attenuation lengths l_t (μm)			
		I	II	III	IV
Chicken fat	200 μm thick (%)	90	118	117	99
Intralipid solution	0.5	570	1250	1046	472
	1.0	409	1000	979	468
	1.5	237	622	797	446
	2.0	198	497	709	433
	20	147	164	323	357

several SWIR regions (1130 to 1260 nm, 1620 to 1820 nm, and 2200 to 2330 nm). Ratios of lipid to protein were used to distinguish stable, vulnerable, and intermediate plaque.[28]

Bone has not been studied previously at wavelengths within window IV. The reduced scattering and absorption coefficients of temporal bones were studied at wavelengths of 635, 690, 780, and 830 nm, but the authors did not go beyond these wavelengths.[29] Likewise, optical properties of the bones in the skull in the range from 650 to 950 nm were investigated, but the authors did not extend their studies to higher wavelengths.[30] In another study, changes in bone density at wavelengths 520 to 960 nm were reported. Again, they did not reach wavelengths in the SWIR range.[31] Pifferi et al. looked at the human calcaneus at different wavelengths between 650 and 1000 nm. They were able to estimate the concentration of key tissue constituents, such as bone mineral, water, lipids, oxy-, and deoxyhemoglobin in human calcaneus, using the absorption spectral profiles of these constituents. It was concluded that the amount of bone mineral matrix decreased in older patients while lipids increased.[32] Others have studied cranial bones at wavelengths extending from 800 to 2000 nm. The absorption spectra

showed major absorption peaks located at 978, 1192, 1745, and 1930 nm. These investigators felt the peaks were secondary to increased lipid content.[33] Although the authors were able to reach wavelengths at the second and third NIR optical windows, they were not able to study window IV.

Numerous studies have utilized noninvasive, NIR, optical techniques to distinguish and to assess diseased versus healthy tissues. One study used light between 610 and 1040 nm to obtain the absorption spectra of benign and malignant breast tissues. Based on the absorption profiles of these tissues, it was found that the collagen and lipid content varied significantly among the patients. Women with highly adipose breasts were found to have relatively little collagen in their breasts, while relatively more collagen was found in women with very small breasts.[34] Another group used light from the visible to the NIR range (500 to 1600 nm) to distinguish breast cancer, benign tumors, and normal tissues, by utilizing comparisons of the relative fractions of collagen, water, and fat. Average lipid volume (%) at areas of normal tissue was 80%, whereas it was only ~10% for carcinoma *in situ* (a very early stage of cancer) and <5% for fibroadenoma or for carcinoma, whereas collagen volume was higher for carcinoma than for fibroadenoma or for adipose tissues.[35] These results were consistent with those we have previously reported, which showed increased tryptophan emission in breast cancer samples compared to their paired normal samples, and revealed higher levels of tryptophan in grade III cancers compared to grade I cancers.[36,37] Since carcinomas of the prostate and breast demonstrate decreased fat content and increased protein content in comparison to their adjoining nonmalignant tissues, the minimal water absorption occurring at window IV may allow better assessment of diseased versus healthy tissue, based on the relative fractions of collagen, water, and fat that are detected.

Wilson et al. have recently reported that the absorption peaks of lipids occur at 920, 1040, 1210, 1730, and 1760 nm.[9] Our study shows that the total attenuation length (l_t) from all tissue samples were significantly longer in the three SWIR windows compared to the conventional first NIR window, despite increased collagen or lipid content. Scattering losses due to the solid angle were the same for all specimens. A single scattering event is likely when l_t is greater than the sample thickness. Total attenuation measurements were evaluated based on the relative absorption measurements from the first NIR window

Table 4 Select chromophores at the first and SWIR optical windows.

Window	Wavelength range (nm)	Chromophores	Absorption peak (nm)
I	650 to 950	Deoxyhemoglobin (Hb)	780
		Oxyhemoglobin (HbO$_2$)	830
II	1100 to 1350	Lipids	1200
		Collagen	1200
III	1600 to 1870	Lipids	1730, 1750
		Collagen	1725
IV	2100 to 2350	Collagen	2300

and the SWIR windows for each tissue. Attenuation lengths obtained from studying lipid rich tissues were longer in the SWIR optical windows (specifically NIR windows II and III) compared to the first NIR window. It is possible that the second and third NIR optical windows are most valuable in studies of tissues with decreased collagen and increased lipid content, whereas windows III and IV might be particularly useful for diagnosis and evaluation of bone diseases or cancer (Table 4).

Attenuation lengths obtained from studying bone tissues were greatest at the longest wavelength range in the SWIR (namely at third and fourth windows). The composition of bone is approximately one-third collagen, and, importantly, bone has very little fat content.[38,39] Collagen has an absorption peak at 2300 nm. It may be that minimal absorption at the fourth window and negligible scattering provides the ideal combination for deep tissue imaging of bone and other collagen-rich tissues. Window IV may also be most valuable for evaluation of other tissues, including cartilage, teeth, blood vessels, intervertebral discs, and skin.

6 Conclusion

Total attenuation lengths (l_t) from cancers, bone, chicken fat, and solutions of intralipid were calculated at the first NIR and SWIR optical windows. l_t results from all tissue samples reveal significantly greater lengths in the three SWIR windows compared to the conventional first NIR window, despite increased collagen or lipid content. Moreover, we note that NIR windows II and III appear to be the optimal SWIR range for studying tissues with a higher fat content, for example, normal breast, brain, and normal prostate. Because of their increased collagen content, cancer and diseases of bone may be best studied at windows III and IV. Among potential medical uses of the fourth window are the evaluation of skin cancers, studies of brain, atherosclerosis and vulnerable plaque, aneurysms, and evaluation of disorders of bone, including Paget's disease and osteogenesis imperfecta. Imaging using the SWIR windows with a compact supercontinuum laser light system (with advantages including high power, broadband spectrum, and the ability to span from the ultraviolet to the infrared) may be utilized in combination with many optical applications including label-free microscopy, fluorescence lifetime imaging, and may also be useful during endoscopy to reveal early and *in situ* cancers.

References

1. C. H. Liu et al., "NIR Raman and fluorescence spectroscopies diagnose cancer," *Proc. SPIE* **1887**, 188 (1993).
2. G. Yu et al., "Near-infrared diffuse correlation spectroscopy in cancer diagnosis and therapy monitoring," *J. Biomed. Opt.* **17**(1), 010901 (2012).
3. B. Shadgan et al., "Wireless near-infrared spectroscopy of skeletal muscle oxygenation and hemodynamics during exercise and ischemia," *Spectroscopy* **23**(5–6), 233–241 (2009).
4. M. Wolf et al., "Progress of near-infrared spectroscopy and topography for brain and muscle clinical applications," *J. Biomed. Opt.* **12**(6), 062104 (2007).
5. E. Keller et al., "Noninvasive measurement of regional cerebral blood flow and regional cerebral blood volume by near-infrared spectroscopy and indocyanine green dye dilution," *Neuroimage* **20**(2), 828–839 (2003).
6. L. A. Sordillo et al., "Time-resolved fluorescence for breast cancer detection using an octreotate-indocyanine green derivative dye conjugate," *Proc. SPIE* **8577**, 857708 (2013).
7. D. C. Sordillo et al., "A novel approach to Paget's disease diagnosis and monitoring using near-infrared absorption spectroscopy," *Proc. SPIE* **8565**, 856566 (2013).
8. H. J. Van Staveren et al., "Light scattering in lntralipid-10% in the wavelength range of 400-1100 nm," *Appl. Opt.* **30**(31), 4507–4514 (1991).
9. R. H. Wilson et al., "Review of short-wave infrared spectroscopy and imaging methods for biological tissue characterization," *J. Biomed. Opt.* **20**(3), 030901 (2015).
10. A. M. Smith, M. C. Mancini, and S. Nie, "Bioimaging: second window for in vivo imaging," *Nat. Nanotechnol.* **4**(11), 710–711 (2009).
11. L. A. Sordillo et al., "Deep optical imaging of tissue using the second and third near-infrared spectral windows," *J. Biomed. Opt.* **19**(5), 056004 (2014).
12. L. Shi et al., "Transmission in near-infrared optical windows for deep brain imaging," *J. Biophotonics* **9**(1–2), 38–43 (2016).
13. R. Nachabe et al., "Estimation of biological chromophores using diffuse optical spectroscopy: benefit of extending the UV-VIS wavelength range to include 1000 to 1600 nm," *Biomed. Opt. Express* **1**(5), 1432–1442 (2010).
14. K. M. Yoo, F. Liu, and R. R. Alfano, "Imaging through a scattering wall using absorption," *Opt. Lett.* **16**(13), 1068–1070 (1991).
15. R. R. Alfano, *The Supercontinuum Laser Source*, 3rd ed., Springer, New York (2016).
16. I. T. Sorokina and E. Sorokin, "Femtosecond Cr^{2+}-based lasers," *IEEE J. Sel. Top. Quantum Electron.* **21**(1), 273–291 (2015).
17. D. C. Sordillo et al., "Fourth near-infrared optical window for assessment of bone and other tissues," *Proc. SPIE* **9689**, 96894J (2016).
18. L. A. Sordillo et al., "Third therapeutic spectral window for deep tissue imaging," *Proc. SPIE* **8940**, 89400V (2014).
19. L. Wang et al., "Ballistic 2D imaging through scattering walls using an ultrafast optical Kerr gate," *Science* **253**(5021), 769–771 (1991).
20. Z. Glasser et al., "The effect of measurement on the ballistic-diffusive transition in turbid media," *J. Biomed. Opt.* **18**(10), 106006 (2013).
21. R. R. Alfano et al., "Light propagation in highly scattering turbid media: concepts, techniques, and biomedical applications," in *Photonics: Scientific Foundations, Technology and Applications*, D. L. Andrews, Ed., pp. 367–412, Wiley and Sons, Hoboken, New Jersey (2015).
22. S. L. Jacques, "Optical properties of biological tissues: a review," *Phys. Med. Biol.* **58**(11), R37–R61 (2013).
23. A. Yaroshevsky et al., "The transition from the ballistic to the diffusive regime in a turbid medium," *Opt. Lett.* **36**(8), 1395–1397 (2011).

24. K. M. Yoo, F. Liu, and R. R. Alfano, "When does the diffusion approximation fail to describe photon transport in random media?" *Phys. Rev. Lett.* **64**(22), 2647–2650 (1990).
25. Z. Q. Zhang et al., "Wave transport in random media: the ballistic to diffusive regime," *Phys. Rev. E.* **60**(4), 4843–4850 (1999).
26. T. L. Troy and S. N. Thennadil, "Optical properties of human skin in the near infrared wavelength range 1000 to 2200 nm," *J. Biomed. Opt.* **6**(2), 167–176 (2001).
27. E. Zamoras-Rojas et al., "Optical properties of pig skin epidermis and dermis estimated with double integrating sphere measurements," *Innov. Food Sci. Emerg. Technol.* **20**, 343–349 (2013).
28. J. Wang et al., "Near-infrared spectroscopic characterization of human advanced atherosclerotic plaques," *J. Am. Coll. Cardio.* **39**(8), 1305–1313 (2002).
29. S. Tauber et al., "Light dosimetric quantitative analysis of the human petrous bone: experimental study for laser irradiation of the cochlea," *Lasers Surg. Med.* **28**(1), 18–26 (2001).
30. M. Firbank et al., "Measurement of the optical properties of the skull in the wavelength range 650-950 nm," *Phys. Med. Biol.* **38**(4), 503–510 (1993).
31. N. Ugryumova, S. J. Matcher, and D. P. Attenburrow, "Measurement of bone mineral density via light scattering," *Phys. Med. Biol.* **49**(3), 469–483 (2004).
32. A. Pifferi et al., "Optical biopsy of bone tissue: a step toward the diagnosis of bone pathologies," *J. Biomed. Opt.* **9**(3), 474–480 (2004).
33. A. N. Bashkatov et al., "Optical properties of human cranial bone in the spectral range from 800 to 2000 nm," *Proc. SPIE* **6163**, 616310 (2005).
34. P. Taroni et al., "Absorption of collagen: effects on the estimate of breast composition and related diagnostic implications," *J. Biomed. Opt.* **12**(1), 014021 (2007).
35. R. Nachabe et al., "Diagnosis of breast cancer using diffuse optical spectroscopy from 500 to 1600 nm: comparison and classification methods," *J. Biomed. Opt.* **16**(8), 087010 (2011).
36. L. A. Sordillo et al., "Optical spectral fingerprints of tissues from patients with different breast cancer histologies using a novel fluorescence spectroscopic device," *Technol. Cancer Res. Treat.* **12**(5), 455–461 (2013).
37. L. A. Sordillo et al., "Differences in fluorescence profiles from breast cancer tissues due to changes in relative tryptophan content via energy transfer: tryptophan content correlates with histologic grade and tumor size but not with lymph node metastases," *J. Biomed. Opt.* **19**(5), 125002 (2014).
38. S. Teitelbaum, "Bone resorption by osteoclasts," *Science* **289**(5484), 1504–1508 (2000).
39. B. Clarke, "Normal bone anatomy and physiology," *Clin. J. Am. Soc. Nephrol.* **3**, S131–S139 (2008).

Diana C. Sordillo is a PhD student in mathematics at Vanderbilt University and a researcher at the Institute for Ultrafast Spectroscopy and Lasers in the physics department at the City College of CUNY. She received her MS degree in mathematics from New York University.

Laura A. Sordillo received her MS degree in physics at CCNY. She is a PhD student in the Department of Electrical Engineering at CCNY. She has developed with others a portable device for assessment of high grade cancers, found there exist four NIR optical windows that can be utilized to image breast, brain and bone, and investigated the key role of tryptophan in cancers and neurological diseases. She is a recipient of the CCNY-MSKCC Graduate Award.

Peter P. Sordillo is an attending physician at Lenox Hill Hospital, where his specialty is the treatment of patients with extremely rare cancers. He also holds graduate degrees in philosophy (causality) and in physics. He is a research consultant at the Institute for Ultrafast Spectroscopy and Lasers in the physics department at the City College of CUNY.

Lingyan Shi is a research scientist at Columbia University. Her current research focuses on metabolic imaging with nonlinear biomedical optics such as stimulated Raman scattering (SRS). Before coming to Columbia University, she was a research associate studying deep brain imaging and drug delivery in brain at the Institute for Ultrafast Spectroscopy and Lasers and biology department, CCNY, where she received her PhD in biomedical engineering.

Robert R. Alfano is a distinguished professor of science and engineering at the City College of CUNY. He has pioneered many applications of light and photonics technologies to the study of biological, biomedical, and condensed matter systems, invented and used in his research supercontinuum and tunable solid state lasers. He has received his PhD in physics from New York University and is a fellow of American Physical Society, Optical Society of America, and IEEE.